J Mol Model (2013) 19:4781–4788
DOI 10.1007/s00894-013-1937-2

ORIGINAL PAPER

Influence of doped nitrogen and vacancy defects on the thermal conductivity of graphene nanoribbons

Haiying Yang · Yunqing Tang · Jie Gong · Yu Liu · Xiaoliang Wang · Yanfang Zhao · Ping Yang · Shuting Wang

Received: 12 April 2013 / Accepted: 3 July 2013 / Published online: 7 September 2013

Abstract A systematic investigation of the thermal conductivity of zigzag graphene nanoribbons (ZGNRs) doped with nitrogen and containing a vacancy defect was performed using reverse nonequilibrium molecular dynamics (RNEMD). The investigation showed that the thermal conductivity of the ZGNRs was significantly reduced by nitrogen doping. The thermal conductivity dropped rapidly when the nitrogen doping concentration was low. Also, the presence of a vacancy defect was found to significantly decrease the thermal conductivity. Initially, as the vacancy moved from the heat sink to the heat source, the phonon frequency and the phonon energy increased, and the thermal conductivity decreased. When the distance between the vacancy in the ZGNR and the edge of the heat sink reached 2.214 nm, tunneling began to occur, allowing high-frequency phonons to pass through the vacancies and transfer some energy. The curve of the thermal conductivity of the ZGNRs versus the vacancy position was found to be pan-shaped, with the thermal conductivity of the ZGNRs controlled by the phonon. These findings could be useful when attempting to control heat transfer on the nanoscale using GNR-based thermal devices.

Keywords Graphene nanoribbons · Nitrogen doping · Vacancy defects · Thermal conductivity

H. Yang
School of Materials Science and Engineering, Jiangsu University, Zhenjiang 212013, People's Republic of China

Y. Tang · J. Gong · Y. Liu · X. Wang · Y. Zhao · P. Yang
Laboratory of Advanced Design, Manufacturing & Reliability for MEMS/NEMS/ODES, Jiangsu University, Zhenjiang 212013, China

P. Yang (✉)
Laboratory of Advanced Design, Manufacturing & Reliability for MEMS/NEMS/ODES, School of Mechanical Engineering, Jiangsu University, Zhenjiang 212013, People's Republic of China
e-mail: yangpingdm@ujs.edu.cn

P. Yang
e-mail: yangping1964@163.com

S. Wang (✉)
School of Mechanical Science and Engineering, Huazhong University of Science and Technology, Wuhan, Hubei 430074, People's Republic of China
e-mail: wangst@mail.hust.edu.cn

P. Yang
Laboratory of Materials and Micro-Structural Integrity, Jiangsu University, Zhenjiang 212013, People's Republic of China

Introduction

Graphene is a monolayer of graphite with a two-dimensional honeycomb lattice structure of sp^2-bonded carbon. Graphene can be stacked in a three-dimensional structure: graphite; it can be curled into one-dimensional carbon nanotubes, and it can also be warped into zero-dimensional fullerenes, so it is the building block of most carbon-based nanomaterials [1–25]. Independent graphene sheets were first prepared by Novoselov and Geim [1] using micromechanical cleavage in 2004. These sheets exhibit exceptional and unique electronic properties, so they have attracted intense attention from researchers in the past few years. The unusual electronic properties of graphene nanoribbons (GNRs) make them a promising candidate for next-generation micro-nano devices. Claire Berger [2] presented a prototype of a transistor device for ballistic transport that utilizes the excellent electronic migration characteristics of GNRs, which may lead to a breakthrough in the development of high-speed computer chips. Given that silicon-based semiconductor technology is approaching its physical limits, new materials to replace silicon in future semiconductor technologies are urgently needed. Graphene could potentially be the ideal material for next-generation carbon-based integrated circuits due to its excellent performance in this context. We know that

failures of electronic devices can mainly be attributed to thermal failures when the integrated circuits are operating. After all, working devices generate a lot of heat, and if that heat cannot be discharged, it will accumulate in the devices, causing the devices to get hotter and hotter. However, the measured values for the thermal conductivity of GNRs reach as high as several thousands of W/mK, among the highest of any known material. Thus, potential applications of GNRs in thermal devices such as thermal transistors and thermal rectifiers have already been conceptualized. S. Ghosh [3] measured the thermal conductivity of graphene using a noncontact technique based on micro-Raman spectroscopy at room temperature, and found that its value was in the range 3,080–5,150 W/mK. However, it is difficult to test the thermal conductivity of GNRs experimentally on the nanoscale. Also, the structures of GNRs may contain defects, further increasing the difficulty of such a test. On the other hand, it is also possible to use simulation based on molecular dynamics (MD) to investigate the heat transfer characteristics of GNRs. Zhixin Guo [4] investigated the thermal conductivity of GNRs using nonequilibrium molecular dynamics (NEMD). They found that the thermal conductivity of GNRs exhibits a significant size effect in that the thermal conductivity increases with GNR length, and the thermal conductivity of zigzag GNRs (ZGNRs) is higher than that of armchair GNRs (AGNRs).

The chemical functionalization of semiconductor materials through the introduction of atoms and functional groups has attracted significant attention as a way to modify their physical, chemical, and mechanical properties. Shih-Kai Chien [5] investigated the influence of hydrogen coverage on the thermal conductivity of typical hydrogen-functionalized armchair graphene. They found that the system exhibits a rapid drop in thermal conductivity with hydrogen coverage. The thermal conductivity of graphene is reduced by introducing hydrogen into the system. Yuyan Shao [6] exposed graphene to nitrogen (N) plasma to obtain nitrogen-doped graphene (N-graphene), and found that N-graphene exhibits much higher electrochemical activity than pure graphene. This excellent electrochemical performance of N-graphene can be attributed to the nitrogen-based functional groups present and the specific properties of graphene. There are currently three ways to introduce nitrogen into graphene: chemical vapor deposition (CVD) [7], electrothermal reactions [8], and treatment with nitrogen plasma [9]. Many scholars have already investigated the electronic properties of N-graphene, but less attention has been paid to the heat-transfer characteristics of N-graphene. Inspired by previous studies, we used RNEMD to investigate the heat-transfer characteristics of zigzag nitrogen-doped graphene. We also studied the influence of a vacancy defect on the thermal conductivity of graphene. The thermal conductivity showed some interesting phenomena when the GNR structure was modified. The changes in the thermal conductivity of graphene were found to be mainly related to the phonon–phonon mean free path and phonon speed. These results imply that it is potentially possible to control the heat transfer of graphene nanoribbons.

Computational methods

In this work, the thermal conductivity of the ZGNRs was calculated using RNEMD [10], in which the heat flux is imposed on the system to form a temperature gradient. This is the reverse of the usual cause-and-effect picture that the temperature gradient is imposed on the system to induce a heat flux. This approach has the advantage of fast convergence of the temperature gradient in a nonequilibrium steady system with a known value for the heat flux. Since our main focus in this study was on the effects of nitrogen doping and vacancy defect location on the thermal conductivity, we only generated the following ZGNRs for all of the calculations performed in the present work: ZGNR length was 15.25 nm and ZGNR width was 2 nm; ZGNRs were symmetrical, and a periodic boundary condition in the axial direction was considered. Two slabs representing the heat source and sink were separated by half a ZGNR length. Following the conventional notation, Fig. 1 shows half the simulation model for the structure of a ZGNR. The simulation box was divided into 60 slabs along the direction of heat transfer, with the first slab acting as the heat sink and the 31st acting as the heat source. The hottest atom (that with the highest kinetic energy) in the first layer (the heat sink) and the coldest atom (that with the lowest kinetic energy) in the 31st layer (the heat source) were selected. The two sets of atoms were paired up and their velocities were exchanged. When the system reaches a steady state, the heat flux created through exchange processes among atoms balances the heat flux in the axial direction. The heat flux J can be calculated by determining the amount of kinetic energy between the two selected layers according to the following equation:

$$J = \frac{\frac{1}{2}\sum_{Ntransfer}\left(m{v_h}^2 - m{v_c}^2\right)}{t_{swap}} \quad (1)$$

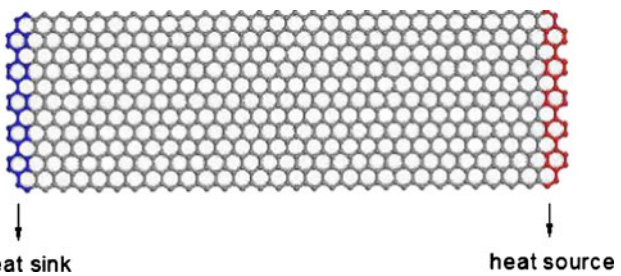

Fig 1 The simulation model of a zigzag graphene nanoribbon (ZGNR)

Table 1 Tersoff potential parameters used for C and N

Parameter	A (eV)	B (eV)	λ ($Å^{-1}$)	μ ($Å^{-1}$)	β	n	c	d	h	R ($Å$)	S ($Å$)
C	1.3936×10^{3}	3.467×10^{2}	3.4878	2.2119	1.5724×10^{-7}	7.2751×10^{-1}	3.8049×10^{4}	4.384	-5.7058×10^{-1}	1.8	2.1
N	1.1×10^{4}	2.1945×10^{2}	5.7708	2.5115	1.056×10^{-1}	12.4498	7.9934×10^{4}	1.3435×10^{2}	−0.9973	2.0	2.3

Interaction (i-j)	χ_{i-j}	ω_{i-j}
C–N	0.9685	0.6381

where t_{swap} and *Ntransfer* are the entire swap time and the number of swaps, respectively, m is the atomic mass, and v_h and v_c are the velocities of the hottest and coldest atoms, respectively. Momentum exchange can be performed every 25 fs under an NVE ensemble. The nonequilibrium steady state can be achieved after 0.5 ns of exchange. The temperature profile was calculated by averaging events across a time interval of 50 ps. The temperature of each slab was calculated based on the Boltzmann equipartition principle, as follows:

$$T_{MD}(islab) = \frac{2}{3Nk_B}\sum_j \frac{p_j^{\,2}}{2m} \tag{2}$$

where $T_{MD}(islab)$ is the temperature of the i th slab, N is the number of atoms in this slab, k_B is Boltzmann's constant, and p_j is the momentum of atom j. The thermal conductivity can be calculated using the Fourier law, as follows:

$$\lambda = -\frac{J}{2A\frac{\partial T}{\partial x}} \tag{3}$$

where A is the cross-section of heat transfer, defined as the width multiplied by the thickness of the ZGNR (the thickness of graphene was assumed to be 0.142 nm, which is the length of the carbon–carbon bond length [11]), and $\frac{\partial T}{\partial x}$ is the temperature gradient along the axial direction of the ZGNR. The temperature jumps at the atomic layer because of mismatched phonon modes between the heat source and the heat sink. The linear part is selected to fit the temperature gradient in calculation. It is worth pointing out that the MD temperature is lower than the Debye temperature (the Debye temperature of graphene is 322 K [12]), so it is necessary to apply quantum correction in the MD approach to obtain accurate results. Below the Debye temperature, quantum effects play an important role in the heat-transfer mechanism for ZGNRs. By assuming that the total system energy is twice the mean kinetic energy at T_{MD} and equal to the total phonon energy of the system at the quantum temperature T_q, the quantum correction is then [13]

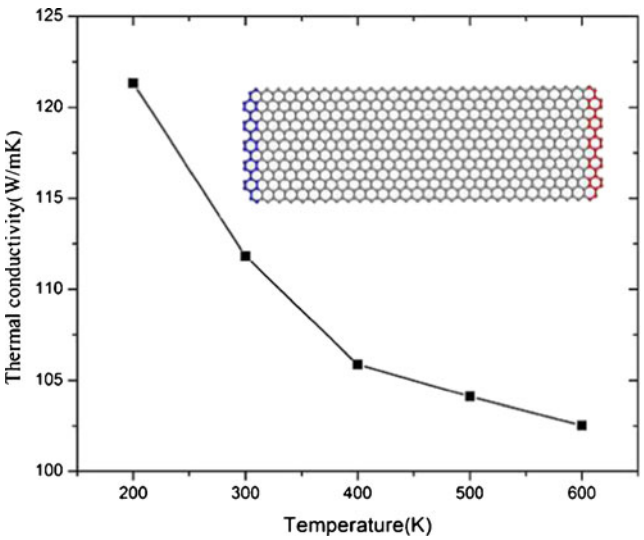

Fig 2 The thermal conductivity of ZGNRs as a function of the temperature

$$m\sum_{i=1}^{N} v_i \cdot v_i = 3Nk_B T_{MD} = \int_0^{\infty} g(w)n(w,T_q)\hbar w dw \tag{4}$$

where $g(w)$ is the density of states, and $n(w,T_q)$ is the following distribution function:

$$n(w,T_q) = \left(e^{\hbar w / k_B T_q} - 1\right)^{-1} \tag{5}$$

where T_q is the quantum temperature, and the distribution function ($n(w,T_q)$) excludes the effect of zero-point energy. The quantum correction is incorporated by multiplying the thermal conductivity (λ) by the ratio dT_{MD}/dT_q [14]:

$$\lambda_q = \left(dT_{MD}/dT_q\right)\lambda \tag{6}$$

where λ_q is the quantum-corrected thermal conductivity.

The phonon spectra function $G(w)$ can be calculated from the Fourier transform of the velocity autocorrelation function as follows [11]:

$$G(w) = \frac{1}{\sqrt{2\pi}}\int e^{-iwt} < \sum_j^N v_j(t)v_j(0) > dt \tag{7}$$

where $v_j(t)$ denotes its velocity at time t and w is the vibration wavenumber.

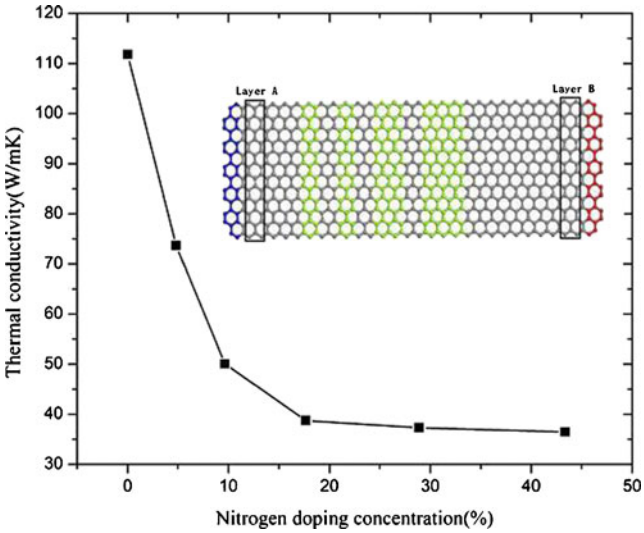

Fig. 3 Thermal conductivity of ZGNRs as a function of the nitrogen concentration calculated at a temperature of 300 K

The velocity Verlet method was employed to integrate the equation. A 0.5-fs time step was used and 1-ns Nose–Hoover thermostat coupling was employed to equilibrate the system. After equilibration, 0.5 ns was used for the NEMD approach and the NVE ensemble. This gave the temperature gradient distribution along the axial direction. In this MD simulation, the velocities were recorded every 10 time steps. The interactions between two atoms (C–C) were described using the second-generation relative empirical bond order (REBO) [15], which incorporates the long-range forces between the atoms. This is a more accurate way to describe the interactions between atoms of the same element; those between atoms of different elements (C–N) were described using the Tersoff potential. Table 1 shows the Tersoff potential parameters for C and N [16, 17].

Results and discussion

To validate our approach, we considered the thermal conductivity of pristine ZGNRs with a length of 15.25 nm and width of 2 nm, as shown in Fig. 1. The thermal conductivity of the ZGNRs was found to be in good agreement with previous simulation results [4]. Some small errors in the simulation results were mainly due to nanoscale size effects and the choice of potential function. As the temperature rose, the thermal conductivity of the ZGNRs showed a gradual downward trend; see Fig. 2. λ was found to be proportional to cvl, where c is the specific heat, v is the speed of sound, and l is the mean free path of phonons. Ballistic heat conduction has limited influence on the linear phonon transport property cv, so the changes in the thermal conductivity are mainly due to variations in the mean free path of phonons. As the temperature rose, this mean free path decreased. As the phonon frequency increased during the heat transfer process, the phonon vibrations got stronger. High-frequency phonons had a greater influence on the heat transfer process, but the scattering of high-frequency phonons is also greater than that for low-frequency phonons, which reduced the heat transfer efficiency of the phonons. Therefore, when the temperature rose, the thermal conductivity of the ZGNRs gradually decreased. These results are similar to those obtained in a previous simulation [18].

The application of nitrogen plasma is a simple and flexible method of obtaining the N-graphene. For example, the nitrogen concentration in the graphene can easily be tailored by changing the plasma strength and/or exposure time. A superlattice of nitrogen-doped graphene can be achieved by adjusting the nitrogen plasma, as shown in the inset in Fig. 3. The concentration of N is $N_0/(N_0+C_0)\times 100$ %, where N_0 is the number of nitrogen atoms and C_0 is the number of carbon atoms [19]. The thermal conductivity is shown as a function of the concentration of N calculated at a temperature of 300 K in Fig. 3. When the nitrogen doping concentration is low, the thermal conductivity drops sharply, especially at concentrations of 0–10 %. When the nitrogen doping concentration is increased from 0 to 10 %, the thermal conductivity falls by 55 %. The structure of the ZGNRs is changed upon the introduction of nitrogen, which results in anharmonic effects on the lattice vibrations. The phonon modes are mismatched during the heat transfer process because of these anharmonic effects, and they also reduce the mean free path of the phonons [20]. The phonons act in a similar manner to continuous plane waves during the transmission process. When a phonon encounters two different materials, the phonon is easily scattered during the resulting phonon mode transformation process. This decreases the heat-transfer capacity of the phonon, so the thermal

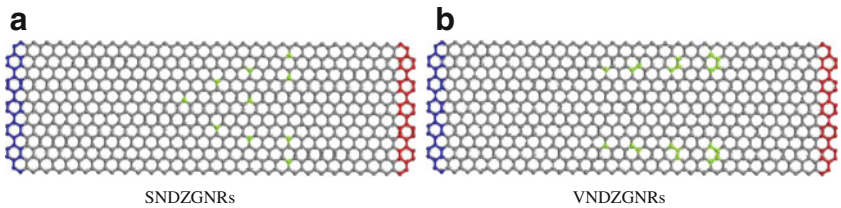

Fig. 4 Different models of nitrogen-doped zigzag graphene nanoribbons

conductivity decreases. Increasing the nitrogen doping concentration gradually decreases the rate of decline of the thermal conductivity of the ZGNRs. The thermal conductivity remains steady when the nitrogen doping concentration increases from 20 % to 43 %. These findings imply that it is potentially feasible to control heat transfer on the nanoscale when designing GNRS-based thermal devices.

Figure 4 shows triangular single-nitrogen-doped zigzag graphene nanoribbons (SNDZGNRs) and parallel various-nitrogen-doped zigzag graphene nanoribbons (VNDZGNRs). Figure 5 shows the thermal conductivities of SNDZGNRs and VNDZGNRs at various temperatures. The thermal conductivity of ZGNRs can be effectively reduced by nitrogen doping. The thermal conductivity of perfect ZGNRs is 112 W/mK, whereas the thermal conductivities of SNDZGNRS and VNDZGNRs are 52 W/mK and 47 W/mK, respectively, which are reductions of 53.6 % and 58 %, respectively, compared to the pure ZGNRs at a temperature of 300 K. SNDGNRs inhibit the heat-transfer process more than VNDGNRs do. The structure of the interface at the location of the nitrogen dopant is that of ZGNR. The temperature jumps at the interface and there is thermal resistance at the interface, and phonons are easily scattered and reflected at the interface during the heat-transfer process. This effectively reduces the thermal conductivity of the ZGNRs [21]. As the temperature rises, the difference in thermal conductivity between SDZGNRs and VDZGRs first increases and then decreases. The difference is smallest at a temperature of 500 K.

In reality, ZGNRs inevitably have defects, and these defects can affect the heat-transfer characteristics. The defects in the ZGNRs can significantly decrease their thermal conductivity [12]. We studied the effect of the location of a defect on the heat-transfer characteristics of the ZGNRs. A single circular vacancy was created by removing all six carbon atoms of a hexagon. Figure 6 shows the thermal conductivity as a function of the location of the vacancy at a temperature of 300 K, as the vacancy moves from heat sink to heat source. At 300 K, the thermal conductivity of the perfect ZGNRs is 112 W/mK, which is significantly higher than the thermal conductivity of the ZGNRs containing a vacancy. When the distance between the vacancy and the edge of the heat sink is 2.214 nm, the thermal conductivity drops by 39 %. The vacancy in the ZGNR hinders phonon transport and decreases the thermal conductivity. A plot of the thermal conductivity of ZGNRs as a function of the location of the vacancy is pan-shaped, as shown in Fig. 6: it is high at both ends and low in the middle. A similar pan shape is found for SiGe nanowires upon tuning the composition [23]. When the vacancy moves from the heat sink to the heat source, the phonon frequency increases around the vacancy. The role of high-frequency phonons in the heat-transfer process is enhanced, while high-frequency phonons are much more easily scattered. Hence, the thermal conductivity decreases when the vacancy moves from heat sink to heat source. As the vacancy continues to move towards the heat source, the phonon frequency and the phonon energy increase. At some point, it becomes possible for the high-frequency phonon to pass through the vacancy via tunneling, meaning that the high-frequency phonon can transfer some energy. At this point, the thermal conductivity begins to rise. These findings are useful, as they suggest that it is possible to control the heat transfer process in ZGNRs by tuning the location of the vacancy in the ZGNRs.

In order to elucidate the mechanism underlying this phenomenon, we proceeded with a detailed analysis of the phonon spectrum at different N concentrations. Figure 7

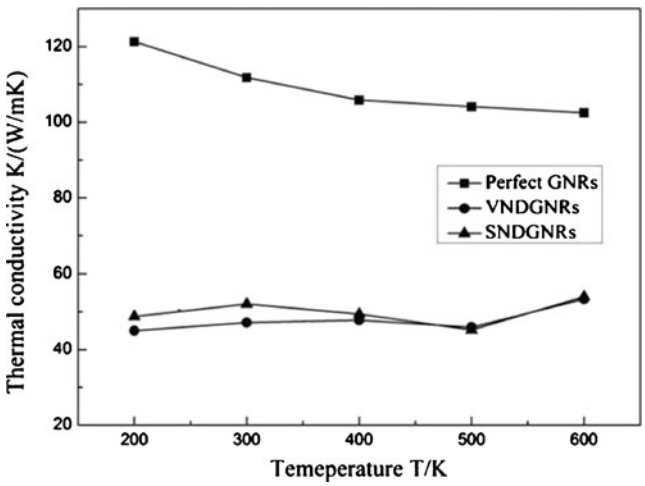

Fig. 5 The thermal conductivities of SNDZGNRs and VNDGNRs as a function of the temperature

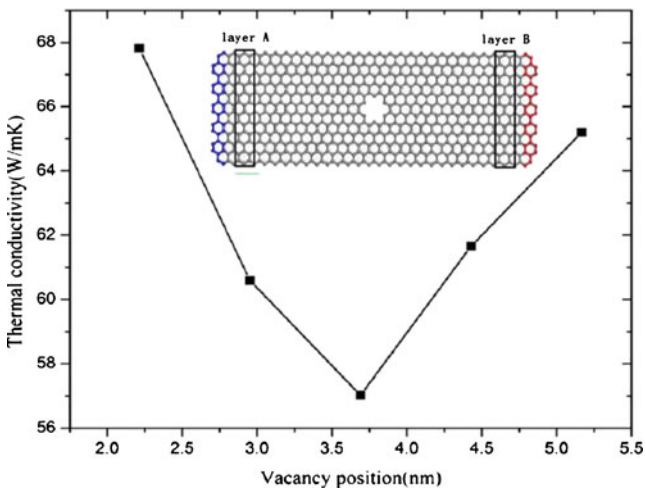

Fig. 6 The thermal conductivity of ZGNRs as a function of the location of the vacancy as the vacancy moves from heat sink to heat source

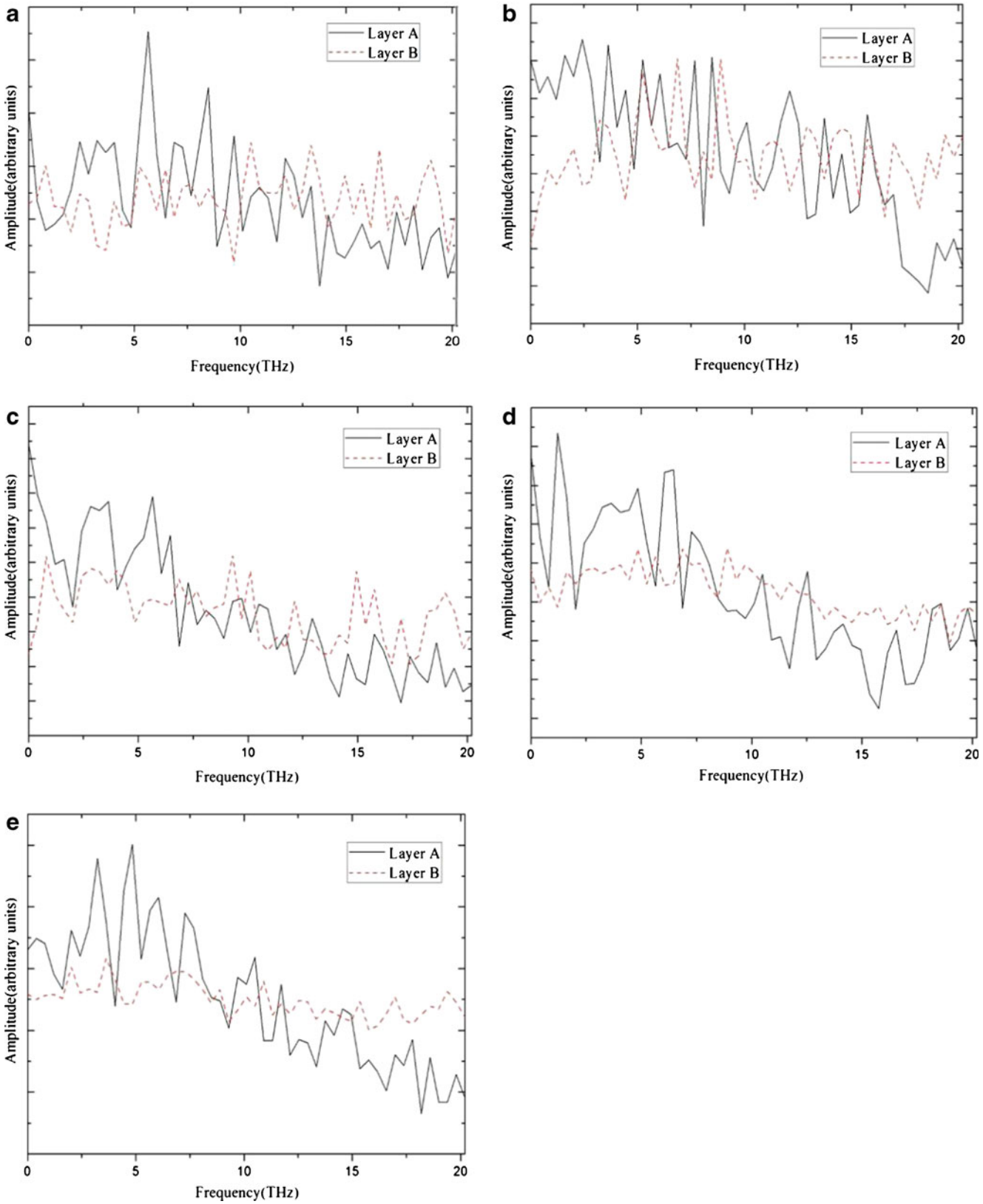

Fig. 7a–e Phonon spectra of NDGNRs at layer A and at layer B and at a temperature of 300 K. **a–e** show the phonon spectra of layers A and B with nitrogen coverages of 4.82 %, 9.63 %, 17.66 %, 28.89 %, and 43.34 %

shows phonon spectra of the A and B layers depicted in the inset of Fig. 3 at different N concentrations. By comparing the overlap of the phonon spectra for the two layers, we can elucidate how the spectra for the two layers match and/or mismatch. It is clear that the phonon spectra overlap significantly when the thermal conductivity is high. A large spectral overlap means that phonons can easily pass through the system, thus resulting in a high thermal conductivity. In order to quantify the above phonon spectral analysis, the overlap (S) of the phonon spectra was calculated as [24]

$$S = \frac{\int_0^\infty P_A(\omega)P_B(\omega)d\omega}{\int_0^\infty P_A(\omega)d\omega \int_0^\infty P_B(\omega)d\omega} \quad (8)$$

where $P_A(\omega)$ is the phonon spectrum of the A layer, and $P_B(\omega)$ is the phonon spectrum of the B layer. According to Fig. 7, S is 0.61397, 0.573266, 0.55688, 0.5188599, or 0.47854 for N coverages of 4.82 %, 9.63 %, 17.66 %, 28.89 %, or 43.34 %, respectively. As the N concentration increases, the phonon modes become increasingly mismatched, so the thermal conductivity decreases. The thermal conductivity of the NDZGNRs is mainly affected by the phonon mode mismatching during the transmission process.

We also calculated S for the phonon spectra of layers A and B at different vacancy locations in the ZGNR. The results are shown in Fig. 8. We found that the curve of the overlap of the phonon spectra is similar to that for the thermal conductivity (shown in Fig. 6). The thermal conductivity of ZGNRs is mainly affected by the phonons. As the mismatch in phonon modes increases, the thermal conductivity decreases. When the vacancy reaches a particular position, S starts to increase, which means that phonons can easily pass through the ZGNRs along the direction of the temperature gradient, so the thermal conductivity rises.

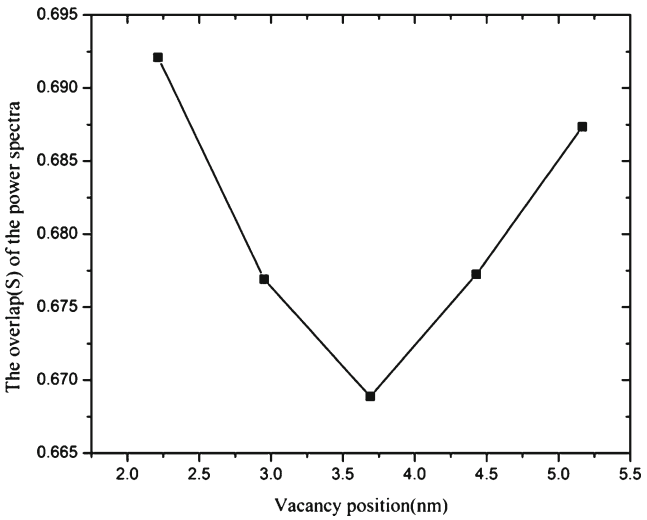

Fig. 8 Overlap (S) of the phonon spectra of layers A and B as a function of the location of the vacancy in the ZGNR at a temperature of 300 K

Conclusions

In this paper, the thermal conductivity of nitrogen-doped ZGNRs and those of ZGNRs containing vacancies at different locations were investigated using RNEMD. The thermal conductivity of ZGNRs containing nitrogen was significantly lower than that of the pure ZGNR. When the nitrogen concentration was low, the thermal conductivity decreased almost linearly as the nitrogen concentration increased. The thermal conductivity at a nitrogen concentration of 10 % was about 55 % lower than that at 0 %. When the N concentration rose above 20 %, the thermal conductivity became less sensitive to nitrogen concentration. Meanwhile, the results also showed that the structure of triangular SNDGNRs inhibits the heat-transfer process more than the structure of parallel VNDGNRs does. The thermal conductivity of SNDGNRs is lower than that of VNDGNRs. Initially, as the temperature is increased, the difference in thermal conductivity between SDZGNRs and VDZGRs increased. This difference then decreased as the temperature rose from 200 to 600 K. This difference was largest at a temperature of 300 K. The presence of a vacancy in the structure of the ZGNRs was found to hinder phonon transmission along the axial direction of the ZGNR. In addition, the curve of the thermal conductivity versus the vacancy position with respect to the heat sink and heat source was pan-shaped. The heat-transfer characteristics of ZGNRs are thus mainly affected by phonon transmission. Less reflection and better matching of phonon modes leads to higher thermal conductivity.

Acknowledgments The authors would like to acknowledge the support of the National Natural Science Foundation of China (61076098, 51275182), the support of the Jiangsu Province Science Foundation for Youths, the Innovative Science Foundation for Graduate Students of Jiangsu Province (CXZZ13_0655, CXLX12_0622), and the Special Natural Science Foundation for the Innovative Group of Jiangsu University during the course of this work.

References

1. Novoselov KS, Geim AK (2004) Science 306:666
2. Berger C, Song Z, Li X, Wu X, Brown N (2006) Science 312:1191
3. Ghosh S, Callizo L (2008) Appl Phys Lett 92:151911
4. Guo Z, Dier Z, Xin-Gao G (2009) Appl Phys Lett 95:163103
5. Chien S-K, Yue-Tzu Y, Chaó-Kuang C (2011) Appl Phys Lett 98:033107
6. Shao Y, Sheng Z, Mark HE (2010) J Mater Chem 20:7491
7. Dacheng W, Yunqi L, Yu W (2009) Nano Lett 5:1752
8. Xinran W (2009) Science 324:768
9. Ying W, Yuyan S (2010) ACS Nano 4:1790
10. Florian Muller-Plathe J (1997) Chem Phys 106:6082
11. Ning W, Langqing X, Hui-Qiong W (2011) Nanotechnology 22:105705
12. Jiuning H, Xiulin R, Chen YP (2009) Nano Lett 7:2730
13. Luks JR, Zhong H (2007) J Heat Transfer 129:705
14. Jiang J-W, Lan J, Jian-Sheng W (2010) J Appl Phys 107:054314
15. Donald WB, Olga AS (2002) J Phys Condens Matter 14:783
16. Tersoff J (1989) Phys Rev B 39:5566
17. Katsuyuki M, Craig F (2000) J Appl Phys 38:L48
18. Nika DL, Pokatilov EP (2009) Phys Rev B 79:155413
19. Hu J, Stephen S, Ajiit V, Xiulin R (2010) Appl Phys Lett 97:133107
20. Yang N, Nianbei L, Lei W (2007) Phys Rev B 76:020301
21. Abramson AR, Tien C-L, A. Majumdar (2002) ASME J Heat Transfer 124:963
22. Chien S-K, Yue-Tzu Y, Cháo-Kuang (2010) Phys Lett A 374:4885
23. Chen J, Zhang G, Li B (2009) Appl Phys Lett 95:073117
24. Baowen L, Lan J, Wang L (2005) Phys Rev Lett 95:104302
25. Yang P, Li X, Yang H, Wang X, Tang Y, Yuan X (2013) Appl Phys Mater Sci Process. doi:10.1007/s00339-013-7607-5